International Journal of Engineering Research & Technology (IJERT)
ISSN: 2278-0181
Vol. 8 Issue 11, November-2019

Where $\mu_0$ is permeability of free-space ($\mu_0 = 4 \times 10^{-7}$H/m), $A_a$ is the cross-section of the air-gap which is assumed to be equal to pole face area, N is the number of turns per pole, G is a nominal air gap between stator and rotor, α is half the included angle of a pole (α =22.5°), $I_b$ is bias current which is kept fixed and $i_n$ (n = 1, 2, 3 and 4) are small variable current of corresponding poles which are varied according to control strategy. For the sake of simplicity currents in the diametrically opposite poles are kept equal in magnitude, but opposite in direction, i.e., $i_1 = -i_3$ and $i_2 = -i_4$. In the actuator design, the allowable displacement of the rotor is considered about one-tenth of the air gap size. At normal point of operation, $i_1=i_2=i_3=i_4=0$ and x=y=0. By expanding with Taylor series and neglecting higher order terms, we get:

$$F_{ax} = \frac{4\mu_0 A_g N^2 I_b cos\alpha}{G^2} i_1 + \frac{4\mu_0 A_g N^2 I_b{}^2 cos^2\alpha}{G^3} x = k_{1a} i_1 + k_{2a} x \quad (8a)$$

$$F_{ay} = \frac{4\mu_0 A_g N^2 I_b cos\alpha}{G^2} i_2 + \frac{4\mu_0 A_g N^2 I_b{}^2 cos^2\alpha}{G^3} y = k_{1a} i_2 + k_{2a} y \quad (8b)$$

Here, $k_{1a}$ and $k_{2a}$ are force-current and force-displacement constants of electromagnetic actuator respectively. Computation of currents $i_1$ and $i_2$ as a function of instantaneous errors is the function of controller.

### *3.1 Design of PD Controller*

To minimize the vibration amplitude of system appropriate magnetic force should applied by the actuator; force should act in the opposite direction of motion and should increase with displacement. As seen from above simplified equations, the magnetic force depends upon the pole winding current of an electromagnet; so by controlling pole winding currents, the system response can be controlled. Proportional-Derivative (PD) control is generally used for faster response. Proportional control increase the control input in proportion to the error e(t) within the acceptable range of error. Derivative control changes the control input in proportion to rate of change of error $\dot{e}$ . Equation of control output of PD controller using proportional and derivative gains $K_p$, $K_d$ can be given as

$$u(t) = K_p e(t) + K_d \dot{e}(t) \quad (9)$$

The controlled output is currents and the error signal. Hence, the control currents for pole pair in horizontal direction ($i_1$) and in the vertical direction ($i_2$) are given as [12]:

$$i_1 = K_p e_x(t) + K_d \dot{e}_x(t) \quad (10\,a)$$

$$i_2 = K_p e_y(t) + K_d \dot{e}_y(t) \quad (10\,b)$$

As the set point is having zero velocity and displacement, the terms $e_x(t) = -x$ and $e_y(t) = -y$ along with $\dot{e}_x(t) = -\dot{x}$ and $\dot{e}_y(t) = -\dot{y}$. Designer has to select the appropriate gain constants $K_p$ and $K_d$ and obtain the control forces $F_{ax}$ and $F_{ay}$.

### *3.2 Neural network based controller*

As seen from Eq.(7), it is observed that the control forces are functions of the velocities of rotor and its radial displacements. The control function in non linear in nature. So, a control concept similar to an inverse dynamic model of the system is used. A nonlinear controller based on trained neural network model with instantaneous transient response as inputs and corresponding currents as outputs is proposed in present work. Fig.5 shows the block diagram of the control methodology.

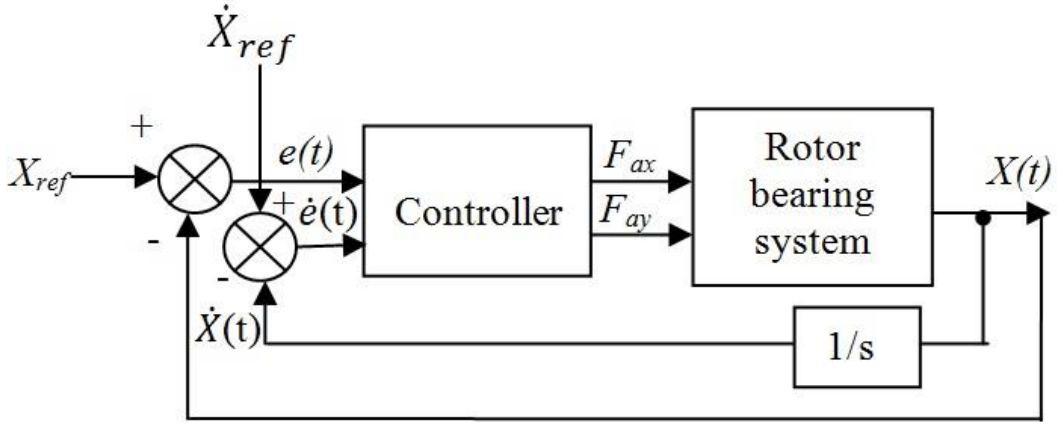


Fig. 5. Error based control scheme.

Conventional 3-layer back propagation neural network is used to train the data. The inputs for the neural network are errors (vector of negative X(t) values) and error rates (vector of negative $\dot{X}(t)$ values) over a sampling period as the values of $i_1$ and $i_2$ are varied randomly from 0 to 100 milli-amperes according to equations (7). A 4 input (*-x*, *-y*, *-ẋ* and *-ẏ*) and two output ($i_1$, $i_2$) training patterns generated inversely have been used in training. Learning rate of 0.4 and momentum

International Journal of Engineering Research & Technology (IJERT)
ISSN: 2278-0181
Vol. 8 Issue 11, November-2019

factor of 0.01 are implemented. Optimum hidden layer nodes were found to be 4 and the neural network is trained using an interactive computer program to find the set of weight matrices. Further, these are employed in estimating the unknown currents corresponding to a computed nodal displacement and velocity vectors during every time step. The detailed backpropagation algorithm for 3-layer multilayer perceptron network can be found in open literature [34].

## 4 RESULTS AND DISCUSSIONS

The coupled set of differential equations is evaluated in time-domain series with aid of Runge-Kutta equation of order four with initial value as zero. The dimensional properties of the rotor used in the analysis shown in Table 1. A speed ratio of 1.5 is implemented between HP and LP rotors. The material for the spools is steel with modulus of elasticity value E=210 GPa and density $\rho$=7.8 g/cm$^3$. All four disks have polar moment of inertia ($I_P$) twice the diametric mass moment of inertia ($I_D$). Further, an eccentricity of 10 microns is considered in the disks. The resultant stiffness, mass, damping (damping factor of 0.01) and gyroscopic matrices are used. The SFD parameters used are [35]: $\mu=5\times10^{-3}$ PaS, $c=2\times10^{-4}$ m, $L=8.3\times10^{-3}$ m, $R_1$=0.03 m. The value of $\omega$ is set as 2000 rpm and angular acceleration $\alpha$ is varied.

Table I Geometric and material data for rotor (Referring to Fig.2)

| Node | Axial dist.(mm) | $d_{outer}$ (mm) | $d_{inner}$ (mm) | Disc mass(kg) | $I_P$ (kg-mm$^2$) |
|---|---|---|---|---|---|
| 1 | 0 | 30.4 | 0 | - | - |
| 2 | 76.2 | 30.4 | 0 | 4.904 | 0.02712 |
| 3 | 323.85 | 30.4 | 0 | - | - |
| 4 | 406.4 | 30.4 | 0 | - | - |
| 5 | 457.2 | 30.4 | 0 | 4.203 | 0.02034 |
| 6 | 508 | 30.4 | 0 | - | - |
| 7 | 152.4 | 50.8 | 38.1 | - | - |
| 8 | 203.2 | 50.8 | 38.1 | 3.327 | 0.01469 |
| 9 | 355.6 | 50.8 | 38.1 | 2.227 | 0.0972 |
| 10 | 406.4 | 50.8 | 38.1 | - | - |

Fig.6 depicts the frequency response plot of a system considering ball bearing forces and not considering the forces. Fig.6(a) coincides well with the available results. It is seen that there are multiple ball passing frequencies (VC) along with harmonics in the system, when ball bearing forces are accounted.

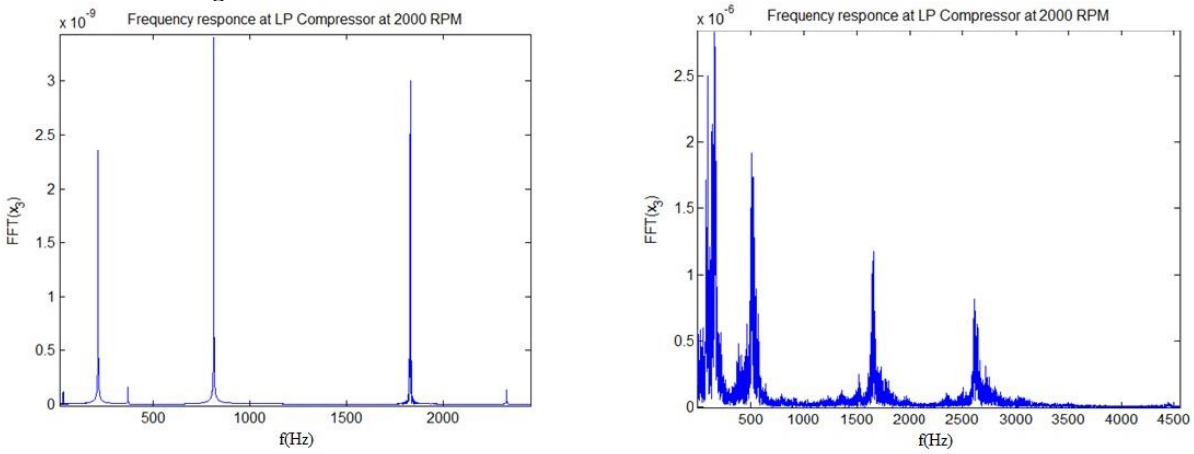


(a) Bearings as spring-damper system (b) Bearings with forces considered

Fig. 6. Frequency plots of rotor at speed of 2000 rpm.

Fig.7 shows the transient analysis results at different acceleration conditions in terms of frequency responses. It is obvious that the multiplicities of ball passing frequencies increase with acceleration of rotor. This may be due to a randomly changing bearing excitation.

International Journal of Engineering Research & Technology (IJERT)
ISSN: 2278-0181
Vol. 8 Issue 11, November-2019

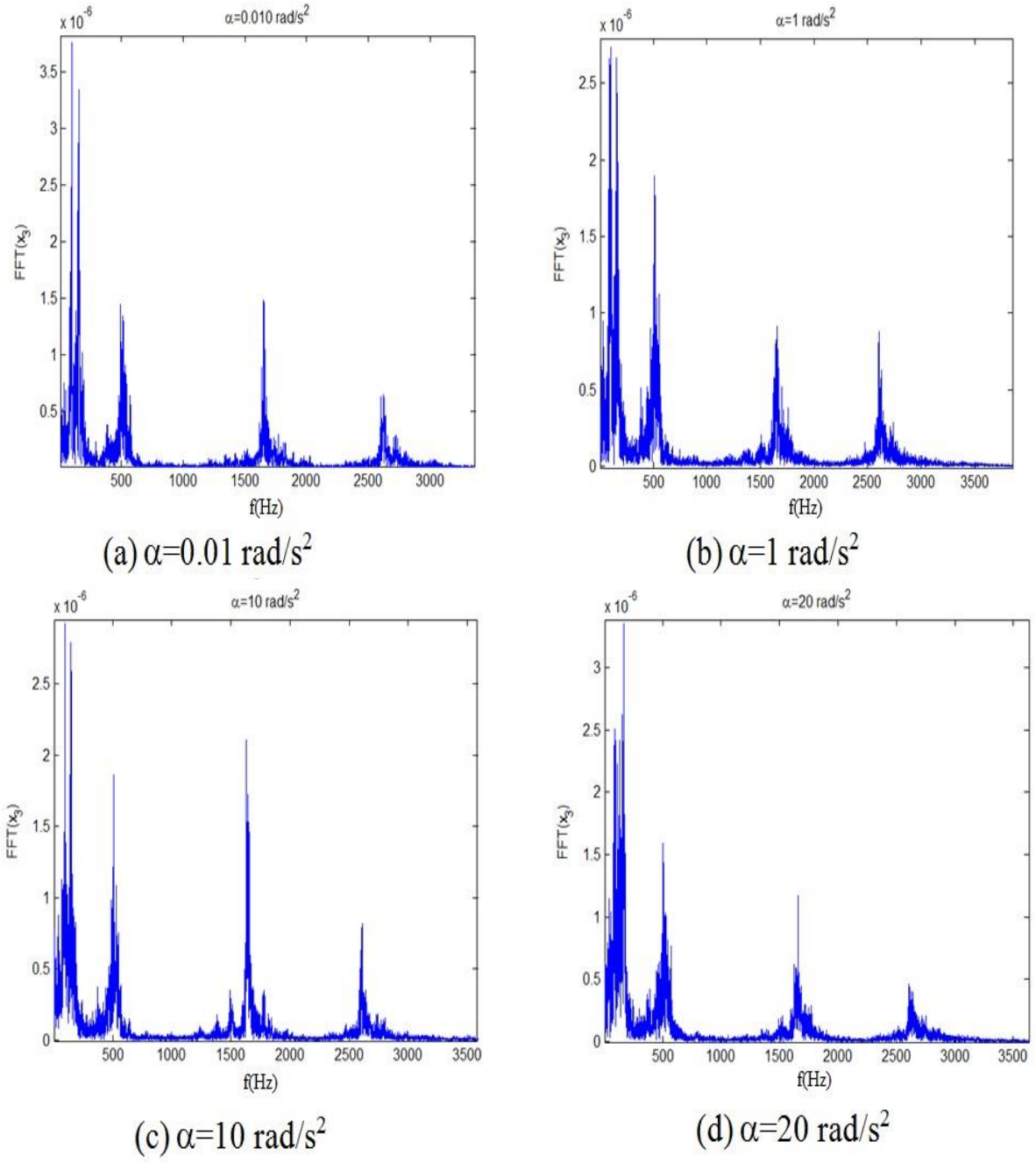


Fig. 7. Effect of acceleration of rotor at LP compressor disk.

In order to minimize the amplitude levels, the following electromagnetic actuator parameters are considered: N=106, G=9 cm ,$A_g$=2.4 $cm^2$, α=22.5°, and $I_b$=3 A. The instantaneous current components $i_1$ and $i_2$ depend on the displacements x and y at the disk node-1. The software code is modified to incorporate an extra component of magnetic force on the force vector at right side located at disk-1 Fig.8 shows the frequency response plots of rotor computed when controlled with bearing force and when uncontrolled with force. It indicates that the amplitudes from second mode have reduced drastically and the ball passing frequency amplitudes have been dropped. The methodology can be extended for other nodes of interest.

International Journal of Engineering Research & Technology (IJERT)
ISSN: 2278-0181
Vol. 8 Issue 11, November-2019

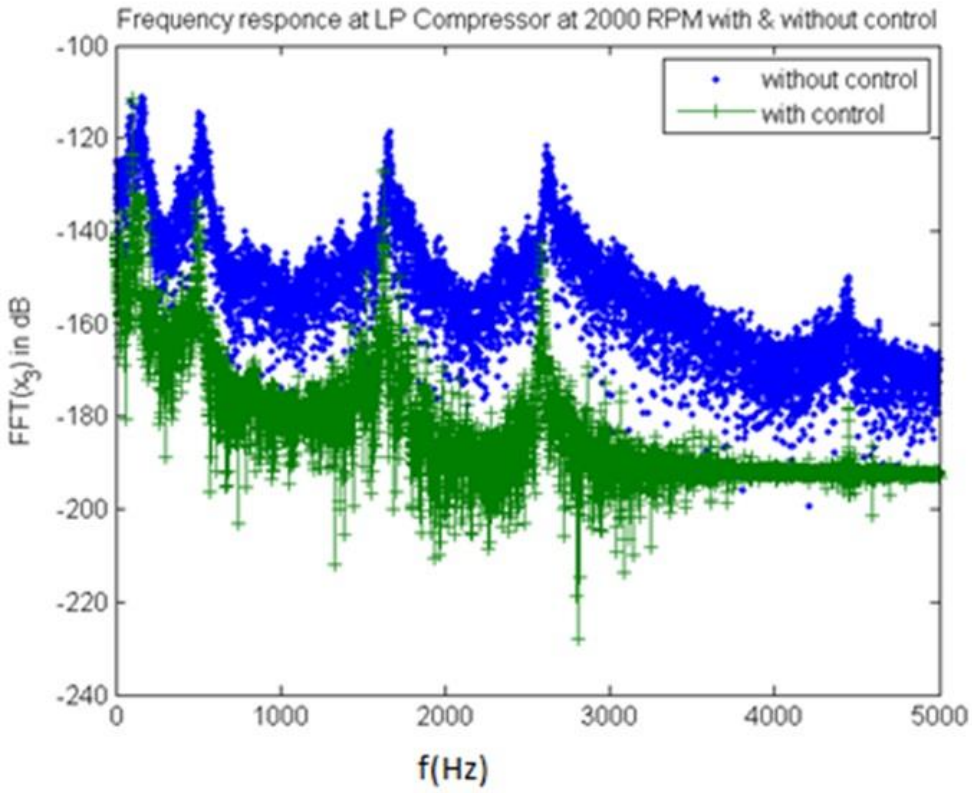


Fig. 8. Amplitude reduction at disk-1 node with EM controller.

## 5 CONCLUSIONS

In current study, a process to reduce vibration with electromagnetic actuators has been briefly presented for a twin-spool rotor case study. The considered system has unbalance and gravity loading along under accelerating conditions. Gyroscopic effects arising due to combined effect of the shaft and disks were accounted, and for all disks unbalance was taken into consideration. Frequency response diagrams were used to distinguish the dynamic response at different angular accelerations of the rotor. It was observed that the squeeze-film damper at the front and rear ends of LP rotor have drastically reduced the amplitudes at critical speeds of operation. Further, the neural-network based electromagnetic actuator designed to provide the nonlinear control forces has considerably reduced the response. Unlike the conventional PD control scheme, the present approach, do not search for optimum set of controller gains. However, it requires huge set of input-output training data before its implementation in the plant. Although the results were illustrated for a selected speed of LP rotor, the focus may be given at the critical speeds of operation in practice so as to identify the effective operational speed range for amplitude attenuation using EM actuator.

## REFERENCES

[1] Zhu C, A disk-type magneto-rheological fluid damper for rotor system vibration control. J Sou Vib 2005;283:1051-1069.
[2] Fan YH, Lee AC. Design of a permanent/electromagnetic magnetic bearing- controlled rotor system. J Fran Inst 1997;334:337-356.
[3] Verichev NN, Verichev SN, Erofeyev VI. Damping lateral vibrations in rotary machinery using motor speed modulation. J Sou Vib 2010;329:13-20.
[4] Zhong J, Li L. Fractional-order system identification and proportional-derivative control of a solid-core magnetic bearing. ISA Trans 2013;
[5] Burrows C, Sahinkaya M, Clements S. Active vibration control of flexible rotors: an experimental and theoretical study. Proc Roy Soc Lon A 1989;422:123-146.
[6] Lin YH, Yu HC. Active modal control of flexible rotor. Mechanical Systems and Signal Processing 2004;18:1117-1131.
[7] Jang MJ, Chen CL, Tsao YM. Sliding mode control for active magnetic bearing system with flexible rotor. J Fran Inst 2005; 342:401-419.
[8] Dimitri A, El-Shafei A. Instability control and unbalance compensation of flexible rotors supported on journal bearings using magnetic bearings. Proceedings of the Eighth IFToMM International Conference on Rotor Dynamics, Seoul, Korea; Sep, 2006. p. 657-664.
[9] Fittro R, Knospe C. Rotor compliance minimization via μ-control of active magnetic bearings. IEEE Trans Con Sys Tech 2002;10(2):238–249.
[10] Riemann B, Perini EA, Cavalca KL, De Castro HF, Rinderknecht S. Oil whip instability control using μ-synthesis technique on a magnetic actuator. J Sou Vib 2013;332:654-673.
[11] Xiaochun G, Dengqing C. Fuzzy proportional-integral-derivative control of an overhang rotor with double discs based on the active tilting pad journal bearing. J Vib Con 2015;19(10):1487-1498.
[12] Fan CC, Pan MC. Active elimination of oil and dry whip in a rotating machine with an electromagnetic actuator. Int J Mech Sci 2011:53:126-134.
[13] Fan CC, Pan MC. Experimental study on the whip elimination of rotor-bearing systems with electromagnetic exciters. Mechanism Machine theo 2011;46:290-304.
[14] Das AS, Nighil MC, Dutt JK, Irretier H. Vibration control and stability analysis of rotor-shaft systems with electromagnetic exciters. Mechanism Machine theo 2008;43:1295-1316.
[15] Das AS, Dutt JK, Ray K. Active vibration control of unbalanced flexible rotor- shaft systems parametrically excited due to base motion. Appli Math Mod 2010; 34:2353-2369.
[16] Das AS, Dutt JK, Ray K. Active control of coupled flexible-torsional vibration in a flexible rotor-bearing system using electromagnetic actuator. Int J Nonli Mechan 2011;46:1093-1109.

International Journal of Engineering Research & Technology (IJERT)
ISSN: 2278-0181
Vol. 8 Issue 11, November-2019

[17] Toha SF, Tokhi MO. A Hybrid Control Scheme for a Twin Rotor System with Multi Objective Genetic Algorithm. 12th International Conference on Computer Modelling and Simulation, Emmanuel College Cambridge, United Kingdom; Mar, 2010. p. 20-28.
[18] Ferfecki P, Zapomel J. Investigation of vibration mitigation of flexibly support rigid rotors equipped with controlled elements. Proc Eng 2012; 48:135-142.
[19] Lin J, Zheng YB. Vibration suppression control of smart piezoelectric rotating truss structure by parallel neuro-fuzzy control with genetic algorithm tuning. J Sou Vib 2012;331:3677–3694.
[20] Qiu ZC. Adaptive nonlinear vibration control of a Cartesian flexible manipulator driven by a ballscrew mechanism. Mech Sys Sig Proc 2012;30:248-266.
[21] Tuma J, Simek J, Skuta J, Los J. Active vibration control of journal bearings with the use of piezoactuators. Mech Sys Sig Proc 2013;36:618–629.
[22] Fang J, Xu X, Tang X, Liu H. Adaptive complete suppression of imbalance vibration in AMB systems using gain phase modifier. J Sou Vib 2013;332:6203-6215.
[23] Han WJ, Chong WL. Proportional-integral-derivative control of rigid rotor-active magnetic bearing system via eigenvalue assignment for decoupled translational and conical modes. J Vib Con 2015; 21(12):2372-2393.
[24] Gunter EJ, Li DF, Barrett LE. Unbalance response of a two spool gas turbine engine with squeeze film bearings. ASME Gas turbine conference and products show, Houston, Texas; Mar, 1981.
[25] Shanmugam A, Padmanabhan C. A fixed–free interface component mode synthesis method for rotordynamic analysis. J Sou Vib 2006; 297:664–679.
[26] Sun G, Palazzolo A, Provenza A, Lawrence C, Carney K. Long duration blade loss simulations, including thermal growths for dual-rotor gas turbine engine. J Sou Vib 2008; 316:147-163.
[27] Hai PM, Bonello P. A computational parametric analysis of the vibration of a three-spool aero-engine under multi-frequency unbalance excitation. J Eng Gas Turb Pow 2011;133:072504-1.
[28] Hai PM, Bonello P. A computational parametric analysis of the vibration of a three-spool aero-engine under multifrequency unbalance excitation. Journal of Engineering for Gas Turbines and Power 2011; 133:072504-1-9.
[29] Lin FJ, Chen SY, Huang MS. Adaptive complementary sliding-mode control for thrust active magnetic bearing system. Con Eng Prac 2011; 19:711-722.
[30] Groves KH, Bonello P, Hai PM. Efficient dynamic analysis of a whole aero engine using identified nonlinear bearing models. Proc Inst Mech Eng, Part C: J Mech Eng Sci 2012;226:66-81.
[31] Chen G. Study of nonlinear dynamic response of an unbalanced rotor supported on ball bearing. J Vib Acou, Trans. ASME 2009;131:061001-1-9.
[32] Inayat HJI, Kanki H, Mureithi NW. On the bifurcations of a rigid rotor response in squeeze-film dampers. J Flui Struc 2003;17:433-439.
[33] Liang MA, JunHong Z, Jiew-Wei L, Jun W, Xin L. Dynamic characteristic analysis of a misaligned rotor-bearing system with squeeze-film dampers. J Zhej Univer-Sci 2016;17:614-631.
[34] Freeman JA, Skapura BM. Neural networks: Algorithms, Applications and Programming Techniques, Addison-Wesley, NY. 1990.
[35] Groves KH, Bonello P. Empirical identification of SFD bearings using neural networks. Mech Sys Sig Proc 2013;35:307-323.